Controlled Morphological Arrangement of Anisotropic Nanoparticles via Oxidation or Ionic Cross-Linking

Marina Rosebrock, Rebecca T. Graf, Daniel Kranz, Hannah Christmann, Hannah Bronner, Adrian Hannebauer, Dániel Zámbó, Dirk Dorfs, and Nadja C. Bigall*

For a long time, researchers in nanochemistry have been exploring ways to create 3D structures using cross-linked nanoparticles, such as lyogels and aerogels. In the present work, how simple modifications to the nanoparticle surface can be used to influence the resulting structure in a targeted manner is demonstrated. Specifically, positively charged surface ligands containing amine groups are compared to negatively charged ligands typically used, containing carboxylic acid groups, to generate network structures using different gelation agents. By utilizing bridging through S^{2-} ions, a network structure of anisotropic CdSe/CdS nanorods is generated, packing them side by side at the nanoscopic level. The resulting structures exhibit improved fluorescence properties comparable to those of tip-to-tip connected networks but without harsh conditions for the nanoparticle surfaces. This innovative new method of gelation using S^{2-} ions can achieve adequate photoluminescence quantum yields as well as prolonged fluorescence lifetimes compared to other network structures.

M. Rosebrock, R. T. Graf, D. Kranz, H. Christmann, D. Dorfs, N. C. Bigall
Institute of Physical Chemistry and Electrochemistry
Leibniz Universität Hannover
30167 Hanover, Germany
E-mail: nadja.bigall@pci.uni-hannover.de

M. Rosebrock, D. Dorfs, N. C. Bigall
Cluster of Excellence PhoenixD (Photonics, Optics and Engineering –
Innovation Across Disciplines)
Leibniz Universität Hannover
30167 Hanover, Germany

M. Rosebrock, R. T. Graf, D. Kranz, A. Hannebauer, D. Dorfs, N. C. Bigall
Laboratory for Nano and Quantum Engineering
Leibniz Universität Hannover
30167 Hanover, Germany

H. Bronner, A. Hannebauer
Institute of Inorganic Chemistry
Leibniz Universität Hannover
30167 Hanover, Germany

D. Zámbó
Institute of Technical Physics and Materials Science
Centre for Energy Research
1121 Budapest, Hungary

The ORCID identification number(s) for the author(s) of this article can be found under https://doi.org/10.1002/sstr.202300186.

1. Introduction

Self-supporting networks such as lyogels and aerogel have gained significant attention in the recent years due to their unique structural,[1–6] optical,[5,7–10] and electronic properties.[8,9,11–19] Among these assemblies, semiconductor nanoparticle networks have been studied for their potential applications in various fields, including sensing.[18,20] The gel formation of semiconductor nanoparticles involves the formation of 3D structures by connecting individual nanoparticles, which can be achieved via various methods such as ligand oxidation,[3,5] cryogelation,[21,22] light irradiation,[6,23,24] or ion-induced assembly.[10,25–28] The resulting assemblies exhibit unique properties, such as enhanced mechanical stability compared to individual nanoparticles, spatial charge-carrier separation after photoexcitation,[8,29–31] and high porosity. These properties are influenced by multiple factors, including the size and shape of the building blocks, the nature of ligands and therefore the surface chemistry, and the method of assembly. By choosing different gelation methods, properties such as fluorescence and thus the efficiency of the charge-carrier transfer can be tuned. Overall, the assembly of semiconductor nanoparticles offers a broad spectrum for the development of novel materials with unique properties and applications overcoming the limitation of solution-based nanocrystals.

This work compares three recently demonstrated gelation methods with a novel technique for linking anisotropic CdSe/CdS nanoparticles: the presented method enables surface ligands to connect nanorods in a side by side and still highly voluminous arrangement. To the best of our knowledge, this is the first time this method has been reported. The new technique is able to cross-link nanorods in this geometrical structure without negatively impacting fluorescence properties such as lowered photoluminescence quantum yields (PLQY), as was observed in, e.g., Ba^{2+}-ion-induced gelation.[10]

In the present work, we give an insight into the importance of choosing the most suitable gelation agent for specific purposes requiring different gel morphologies. As recent studies have mostly dealt with ion-induced gelation,[26,27,32] this work compares the influence of various gelation agents (demonstrating oxidative and non-oxidative gelation treatments) on the structure and property of the nanoparticle gel networks. The gelation of

the building blocks is initiated in aqueous medium and external trigger, namely via the addition of H_2O_2, YCl_3, $BaCl_2$, or Na_2S. The morphology of the resulting network structures is discussed in detail with regard to their optical properties.

The concept of gelation enables the synthesis of desired nanocrystals with tailored properties prior to their assembly into porous, functional gel structures. Since the connection between the building blocks plays a crucial role in the appearance and extent of synergistic properties, our aim is to support the selection of the destabilizing agent and to provide a low-cost and reproducible synthesis pathway toward nanoparticle assemblies.

We found that the selection of gelation agent (i.e., chemically etching the surface or bridging the ligands) drastically influences the nano- and microstructure of the prepared gel networks: while chemical etching (H_2O_2, Y^{3+}) connects the particles leading to a preferential tip-to-tip connection of the elongated building blocks, bridging ions (Ba^{2+} within the mechanism, S^{2-} in the resulting structure) tend to form side-by-side arrangement within nanorod networks. The trend is actually demonstrated for bivalent ions such as Ba^{2+}, Ca^{2+}, and S^{2-}.[10] While the application of other bivalent cations such as Cd^{2+} or Zn^{2+} might also lead to the network formation, the effect of these cations on the photophysical properties of the formed gel networks must be investigated in detail. In our previous publication,[10] we proposed a possible gelation mechanism of bi- and trivalent ions. Briefly, based on the transmission electron microscopy (TEM) images of S^{2-}-gelled samples, in which a distance between the individual nanoparticle building blocks can be seen, we also assume here that the ligands are bridged by the ions. The detection of sulfur in the system between the ligands is however challenging, since sulfur is a component of both the CdS shell and the respective thiolated ligands.

2. Results and Discussion

Figure 1 gives an overview of the samples investigated. Figure 1A shows the samples in UV light from colloidal solutions in a two-phase system to show the transfer from nonpolar to polar media by ligand exchange. The synthesis is performed in nonpolar solution, where particles are covered with trioctylphosphine oxide (TOPO) ligands. Two different ligands were used for phase transfer to aqueous media, namely 3-mercaptopropionic acid (MPA) and 2-dimethylaminoethanethiol (DMAET). MPA contains a thiol group, which is likely bound to the CdS surface of CdSe/CdS nanorods (NR), and a carboxylic acid group, which endows the particles with electrostatic stabilization by their deprotonation in basic conditions. The resulting charge of the carboxylic acid group prevents colloidal nanoparticles from aggregation due to repulsive forces between equal charges. The zeta potential of these colloids is -35.1 ± 1.9 mV. Another part of the same solution from nonpolar solvent is treated with DMAET ligands to obtain a functional diethylamino group instead of a carboxylic acid group. This amino group is positively charged in slight acidic solution and the nanorods have a zeta potential of $+44.8 \pm 1$ mV in these conditions, which also prevent particles from aggregation. The gelation to lyogels (Figure 1) is triggered by various gelation agents, namely H_2O_2, YCl_3, and $BaCl_2$ for MPA-coated NR samples, and Na_2S in case of DMAET-grafted colloidal solution. Lyogels are defined as nanoparticle networks with solvent inside the pore system. Samples with MPA ligands contain water within the pores after gelation and were called hydrogels, samples from DMAET contain ethanol inside the pore system and were called alcogels (both systems can be classified as lyogels). It is very important to mention for alcogels of CdSe/CdS from DMAET samples, that purification with water will induce reversible dissolution of the network structure to colloidal solutions. The mechanism of the reversibility has to be addressed in the future.

Figure 2 shows the structure of the obtained aerogels measured by scanning electron microscopy (SEM). The open porosity of the samples, which is created by the hyperbranched arrangement of CdSe/CdS nanorods, is clearly visible. The SEM images reveal significant differences between the samples. It should be noted that all network structures are produced from the same batch of CdSe/CdS nanorods. Therefore, the building blocks
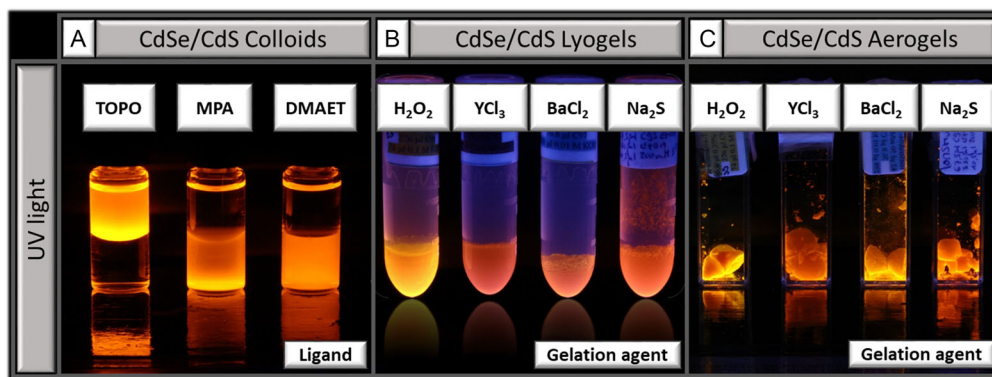

Figure 1. Overview of the discussed samples. Photographs with UV light irradiation of CdSe/CdS nanorods, A) the colloidal solutions (left) before, and (middle and right) after water transfer with mercaptopropionic acid (MPA) and 2-dimethylaminoethanethiol (DMAET), the predominant ligands being indicated in the label above the sample. Colloidal solutions are in a two-phase system: upper part represents the unpolar phase containing toluene, the lower part contains aqueous solution (basic conditions for MPA and slight acidic conditions for DMAET ligands). B) Lyogels, which are filled with water in case of H_2O_2, YCl_3, and $BaCl_2$; Na_2S sample is filled with ethanol and C) aerogels of the samples investigated. The respective gelling agent is mentioned earlier in each sample. H_2O_2, YCl_3, and $BaCl_2$ for the MPA sample, Na_2S is applied in case of the DMAET sample.
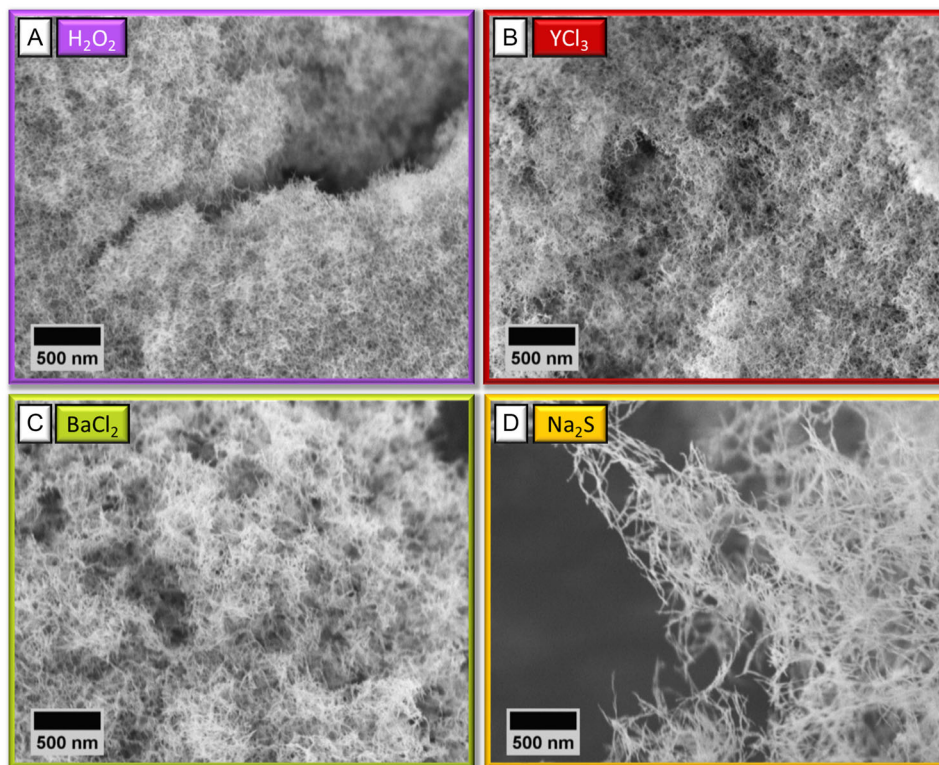
Figure 2. Scanning electron microscopy (SEM) images of aerogels from CdSe/CdS (MPA) with A) H_2O_2, B) YCl_3, C) $BaCl_2$, and CdSe/CdS (DMAET) with D) Na_2S.

are identical in shape and size according to their size distribution (see Figure S2, Supporting Information). The resulting structure is influenced by the choice of ligand and appropriate gelation agent. The network formation with H_2O_2 (Figure 2A) leads to sponge-like structures that exhibit visual homogeneity with SEM. Larger cracks in the structure are probably caused by the handling of the samples during preparation prior to the SEM measurement. Networks produced with YCl_3 (Figure 2B) have a similar, branched structure to those synthesized with H_2O_2. Here, a filigree cross-linked morphology of the material is recognizable. In comparison, gels formed with $BaCl_2$ (Figure 2C) have a slightly more compact arrangement of building blocks, although strong similarities exist at the microscale. In contrast to the images shown in Figure 2A–C, the differences in the arrangement of CdSe/CdS in this network can be seen when using Na_2S (Figure 2D) for gelation. The individual nanorods exhibit greater parallelism in their alignment to each other, resulting in areas with a larger pore volume. The structure can be described as significantly more open and filigree. Images obtained by TEM in **Figure 3** allow for a more detailed examination of the connection points between the nanoparticles (for TEM of pristine colloidal nanoparticles see Figure S2, Supporting Information). It can also be seen that the gelling agent has a significant influence on the way the particles are arranged into the network. TEM images also reveal only slight differences between H_2O_2- and YCl_3-gelled networks (Figure 3A,B). The structure is dominated by tip-to-tip

arrangements of the CdSe/CdS nanorods. It can be observed that the overall network is very disordered, but parallel arrangements of the nanorods to each other are also present. Despite the 2D projection of the 3D samples in the TEM images, the open pore structure of the networks can be observed. In comparison, the network samples gelled with $BaCl_2$ or Na_2S exhibit distinct differences in the arrangement of the particles. These exhibit predominantly a side-by-side arrangement, although they are still assembled into a highly porous and highly voluminous structure. In the case of the $BaCl_2$-gelled network (Figure 3C), the rods are randomly arranged mainly in parallel. The Na_2S-gelled samples (Figure 3D) exhibit the highest degree of order among all samples. It is clear that the nanorods preferentially arrange along their side regions having larger contact area, and this structure is visible throughout the sample. TEM micrographs of aerogels can be seen in Figure S3, Supporting Information. The overall structure is not influenced by the supercritical drying process from lyogels to aerogels. Junction points are similar to those of the hydrogel samples. There is no difference in the overall arrangement of the nanoparticles within the structure upon supercritical drying.

Figure 4 depicts the results from optical spectroscopy measurements performed on colloidal solutions, lyogels, and aerogels. Absorption spectra can be found in Figure S1, Supporting Information. The experimental decay curves (Figure 4A) for fluorescence lifetimes (FLTs) of all corresponding samples were fit
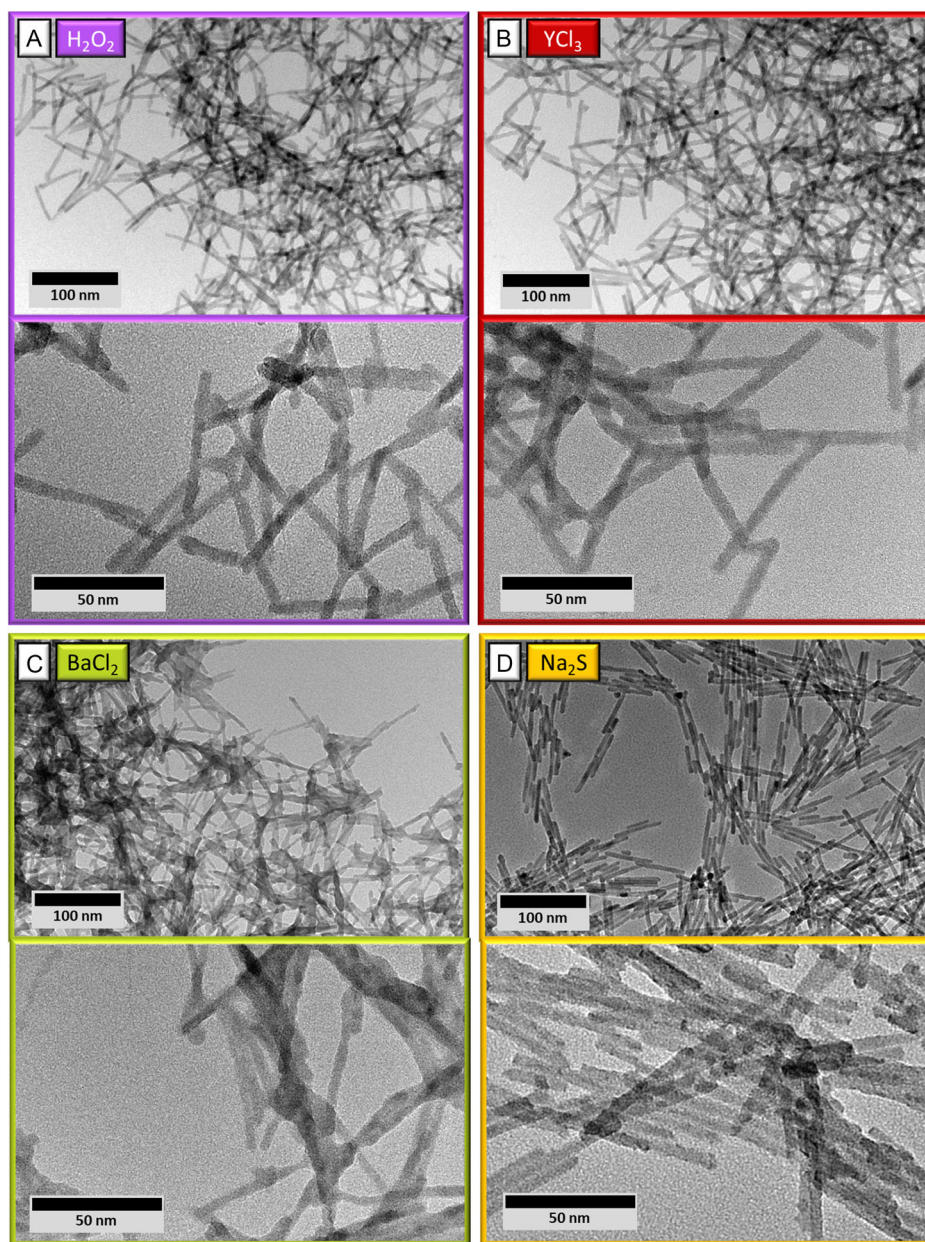
Figure 3. Transmission electron microscopy (TEM) micrographs of lyogels obtained from CdSe/CdS (MPA) with A) H_2O_2, B) YCl_3, C) $BaCl_2$, and CdSe/CdS(DMAET) with D) Na_2S.

monoexponentially (values are given in the text and in Table S1, Supporting Information). These curves were collected at the emission maximum of the corresponding sample and irradiated with a 445.1 nm pulsed light emitting diode (LED) laser. The colloidal solutions, which underwent phase transfer with DMAET or MPA, exhibit a relatively constant lifetime at 26.5 ± 0.1 ns. However, the lyogels differed with respect to their gelation agent. As the result of network formation, gels from H_2O_2 and $BaCl_2$ exhibit faster recombination compared to the initial colloid. In contrast, for the YCl_3 gel, the opposite was observed, while in case of Na_2S gels, only a minor change compared to the initial colloid can be observed. For aerogels, except for the Na_2S gel,

which showed an increase in FLT, the FLT values remained more or less at the level of the initial colloidal solution for the samples gelled with H_2O_2, YCl_3, and $BaCl_2$. The PLQY values in Figure 4B were measured in an integrating sphere in absolute mode and a 445 nm irradiation wavelength. The phase transfer to aqueous media and ligand exchange result in decreasing PLQY values in both cases (MPA and DMAET result in around 21% and 19%) compared to the colloidal solution in unpolar media (TOPO with around 31%). The lyogel formation leads to an additional decrease, where the yield depends on the type of gelling agent used. Upon drying the lyogels, most of them show an increase in PLQY, except from YCl_3-gelled networks, which
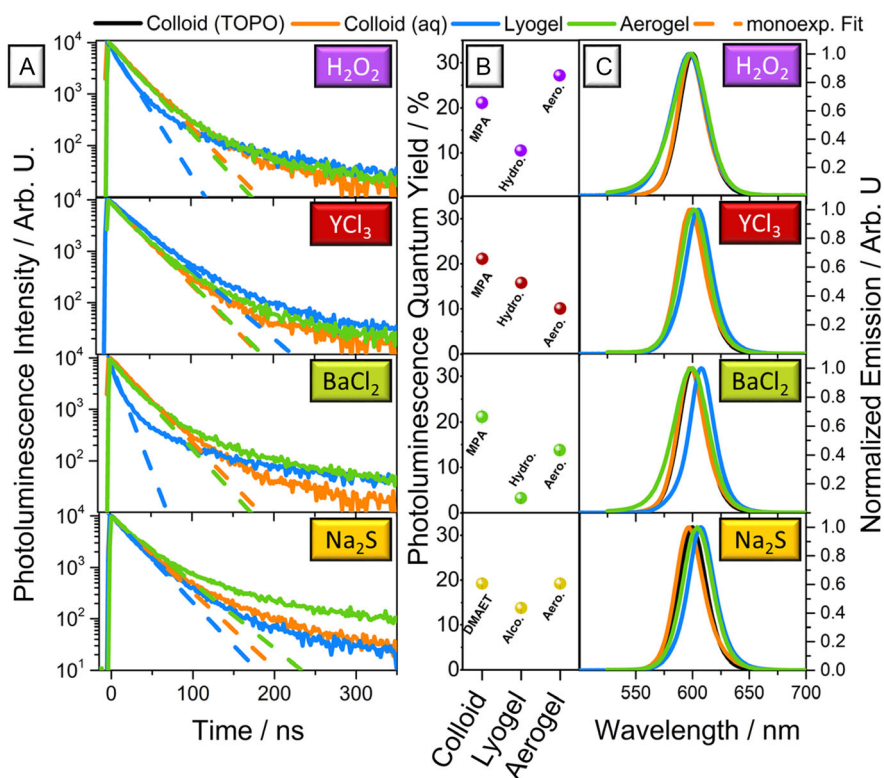
2300186 (4 of 9)

ADVANCED
SCIENCE NEWS
www.advancedsciencenews.com

small
structures
www.small-structures.com

Figure 4. Results from optical spectroscopy measurements. A) Decay curves of all corresponding samples from CdSe/CdS(MPA) with H_2O_2, YCl_3, and $BaCl_2$; CdSe/CdS (DMAET) with Na_2S. B) The values for photoluminescence quantum yield (PLQY) to illustrate the trend from colloid to lyogel to aerogel. C) Normalized fluorescence emission spectra.

decrease relatively by 30%. Samples from H_2O_2 network formation increase by a factor of around 3 due to supercritical drying. Figure 4C shows normalized emission spectra of the corresponding samples. Exact values for emission maxima and full with at half maximum can be found in Supporting Information (see Table S1, Supporting Information). The peak positions stay mostly constant with slight shifts due to network formation, which can be attributed to Förster resonance energy transfer mechanism of the CdSe/CdS,[33] when nanoparticles get in contact and the distance is reduced due to network connection.

These results can be explained as follows. Ligand exchange is always accompanied by surface modification. When the surface is modified in case of the phase transfer from hydrophobic media to aqueous solution, ligands and defects are able to generate new electronic states within the bandgap of the semiconducting material.[34–36] Trap states generated by this treatment can force non-radiative pathways through excited electrons and holes within the excited structure.[37] In addition, the surface ligands themselves can be either acceptors or donors of charge carriers.[33,38] For all measured colloidal samples in aqueous solution (namely CdSe/CdS (MPA) and CdSe/CdS (DMAET) nanorods), the PLQY is decreasing compared to the initial colloid in hydrophobic solution (toluene) due to the aforementioned relationships. In case of FLT, the values are higher for both the CdSe/CdS (MPA) and CdSe/CdS (DMAET) nanorods compared to the original CdSe/CdS (TOPO) sample. Excited electrons can be trapped by the new electronic states within the

ligands, leading to extinction of fluorescence as mentioned earlier, but also to conditions where the electrons take longer until they recombine radiatively or non-radiatively.

Performing gelation in aqueous media, nanoparticle surfaces were differently involved into the process, depending on the interaction of the gelling agent and the surface. In case of H_2O_2 and YCl_3, surface ligands were oxidized by this treatment and ligands where ripped off preferentially at the tips of the anisotropic CdSe/CdS nanorods.[5,8,9] While H_2O_2 is decomposed by oxidizing the surface ligands and possibly the CdS surface itself, YCl_3 residues can be found in the resulting network structures, as we showed in our former publications.[9,10] For side-by-side arranged nanoparticle networks, the PLQY is decreasing as well. The strongest decrease in PLQY can be observed for $BaCl_2$-induced hydrogel formation. This can partially be explained by the dense structure of the resulting network, which is able to reabsorb emitted light from the semiconductor network due to shadowing effects from the side-by-side arrangement of the nanoparticles, i.e., larger apparent particle concentration in the excited volume. The FLT of lyogel samples decreases as a result of network formation when there are no components present that were not originally part of the structure. Specifically, in such samples, the decomposition of H_2O_2 and the washing out of $BaCl_2$[10] from the hydrogel network contribute to the absence of foreign components. Additionally, the presence of Na_2S in the form of S^{2-} is not considered as foreign component for the particles. The reason behind this is mainly the contact between the

**ADVANCED
SCIENCE NEWS**

www.advancedsciencenews.com

**small
structures**

www.small-structures.com

particle surface and the solvent, which quenches the fluorescence by non-radiative processes homogeneously. As a result, only radiative recombination processes take place within the particle, which occur within a very short period of time, visible in the shortened FLT. Post-aging processes in the YCl$_3$-treated samples lead to additional etching of the CdSe/CdS surface,[9,10] which leads to loss of surface ligands.[9] Charge carriers have longer diffusion rates in the material due to the presence of the surface defects before recombining with emissive light radiation.[39]

Lyogels were dried in a specific way to obtain aerogels. For this, the solvent in the pores of the network is gradually exchanged by acetone, and later on dried acetone, to ensure complete miscibility with liquid CO$_2$. Using liquid CO$_2$ as the inner pore solvent is a crucial step to overcome capillary forces against the network structure by raising temperature and pressure within an autoclave to the critical CO$_2$ phase. After the release of the critical CO$_2$ phase, highly porous network structures of the as-prepared gels were obtained. The resulting structures were spectroscopically characterized as before for colloids and lyogels.

Aerogels without residual components from gelation agents (H$_2$O$_2$, BaCl$_2$, and Na$_2$S, see previous section) show increasing PLQY in comparison to lyogels. The main cause of this is likely the absence of solvent molecules, which are effective in quenching the radiative processes. Due to that reason, the PLQY increases compared to the corresponding lyogels. This effect is discussed in detail in our former publication.[5] However, in case of H$_2$O$_2$-gelled networks, the PLQY is obtained with values near the initial colloid in hydrophobic solution, which was already observed in our former publication[8] and is different to the observations of Sanchez-Paradinas et al.[5] The differences originate from different treatment of the phase-transferred colloidal solution. While excess of organic molecules is reduced by an additional washing step with chloroform (see Experimental Section) in this and the former work,[8] Sanchez-Paradinas et al. have refrained from further washing. As a result, oxidation of particles without excess organic components in solution is much more pronounced to the particle surface, which leads to an PLQY value similar to the initial colloidal solution.[5] In addition to the PLQY, the FLT are also increasing at the same time. The extension of FLT in aerogels compared to initial colloidal solutions has previously been discussed to be caused by the particle contacts, which enable the electron transfer through the CdS shell of CdSe/CdS nanorod particles.[5,7,8] In contrast, PLQY of YCl$_3$-gelled networks decrease relatively upon supercritical drying by around 30%. One possible cause may be the nature of the Y component in the system, which has been shown to remain in the structure even through it is washed several times with water and subjected to the drying process.[10,27] The generation of more trap states can lead to higher quenching rates, however, this can be suppressed *via* using reduced amount of YCl$_3$ in the gelation process. However, the absence of solvent outside the network appears to change the environment for electrons such that non-radiative recombination processes become more favorable. Furthermore, the FLT decreases as well, so that a homogeneous quenching process can be assumed. In summary, the S^{2-} system represents a significant advancement for nanoparticle gelation, as it allows for gentle gelation conditions that prevent nanoparticle etching. This results in advantageous photophysical properties that are unique to side-by-side arranged nanorod gels.

3. Conclusion

The nature and type of the substance used to cause gelation play a crucial role in affecting the properties and organization of the resulting nanoparticle network. The electric charge of the molecules that attach to the nanoparticles, along with the appropriate gelation substance, greatly affects the arrangement of the nanoparticles in the network. This study demonstrates that the bridging mechanism essentially governs the particle arrangement. By using negatively charged ligands (MPA) along with H$_2$O$_2$, or positively charged Y^{3+} ions, the particles are able to link tip-to-tip with a preference. Conversely, using Ba^{2+} ions results in a preference for side-by-side arrangement. However, when negatively charged S^{2-} ions are mixed with particles that have positively charged DMAET ligands, the resulting network has also side-by-side arrangement with improved properties compared to the Ba^{2+} system in terms of fluorescence emission and lifetimes. As an aerogel, it shows particularly long FLTs compared to the other aerogel systems (from H$_2$O$_2$, YCl$_3$, and BaCl$_2$). Also, the PLQY are high in this side-by-side nanorod arrangement compared to the same arrangement within the BaCl$_2$ gelled systems. In addition to improved optical properties, samples consisting of CdSe/CdS (DMAET) in combination with S^{2-} ions form a more open-pored structure compared to all other samples. This will lead to a greater accessibility of the individual building blocks for solvent or gas molecules. These structural differences in the resulting network can easily be controlled and adapted for various potential applications. In a certain way, the sample gelled with S^{2-} stands out for side-by-side arranged particle networks. The work thus demonstrates a simple way to arrange nanorods in a controlled manner to form highly porous structures that exhibit particular fluorescence properties. These results can be applied in future work to other systems that require a chemically mild gelation method.

4. Experimental Section

Chemicals: TOPO (99%), sulfur (S, 99.98%), 1-octadecene (ODE, 90%), MPA (99%), yttrium (III) chloride hexahydrate (Y^{3+}, 99.9%), barium chloride dihydrate (Ba^{2+}, 99%), potassium hydroxide (KOH, 85%), ethanol absolute (99.8%), acetone (99.5%), and methanol (99.8%) were purchased from Sigma Aldrich. Tri-*n*-octylphosphine (TOP, 97%) was purchased from ABCR. Cadmium oxide (CdO) and selenium (Se, 99.99%) were purchased from Alfa Aesar. Hexylphosphonic acid (HPA, 99%) and octadecylphosphonic acid (ODPA, 99%) were purchased from PCI Synthesis. Toluene (99.9%) was purchased from Merck Millipore. Acetone extra dry (99.8%) and DMAET hydrochloride (DMAET<img1/>HCl, 95%) were purchased from Acros. Sodium sulfide (Na$_2$S, >99.7%) was purchased from Fisher Scientific. All chemicals were used as purchased and without further purification.

Synthesis of CdSe Seeds: CdSe seeds were prepared following the procedure described by Carbone et al.[40] In a typical synthesis, a mixture of CdO (0.06 g, 0.47 mmol), ODPA (0.28 g, 0.84 mmol), and TOPO (3.0 g, 7.76 mmol) was heated under vacuum at 150 °C. After 1 h, the atmosphere was changed to argon and the mixture was heated to 300 °C to dissolve the CdO, resulting in a clear solution. TOP (1.8 mL, 4.04 mmol) was then added, and the mixture was heated to 380 °C. At this temperature, a mixture of TOP (1.8 mL, 4.04 mmol) and Se (0.058 g, 0.73 mmol) was injected into the flask. The reaction was quenched after 4 min by injecting ODE (4 mL) and removing the heating mantle. The flask was cooled down to 90 °C and toluene (5 mL) was added. The particles were then

precipitated with methanol (8 mL), centrifuged (10 min, 8000 rcf), and redissolved in hexane (8 mL) for purification. This step was repeated twice, and the particles were finally stored in toluene (2 mL). The concentration of the seeds was determined from the absorption spectrum.[41]

CdSe/CdS Dot-In-Rod Particles: This synthesis followed the seeded-growth method.[40] CdO (0.36 g, 2.82 mmol), HPA (0.48 g, 2.88 mmol), ODPA (1.68 g, 5.04 mmol), and TOPO (18 g, 46.56 mmol) were combined in a flask and heated under vacuum at 150 °C for 1 h. After degassing, the atmosphere was switched to argon and the reaction solution was heated to 300 °C until a clear solution was obtained. TOP (3.6 mL, 8.08 mmol) was injected into the flask, and the synthesis solution was heated to 350 °C. The prepared CdSe nanoparticles (0.48 µmol) in hexane were dried with an ambient air flow and then redissolved in a mixture of TOP and sulfur (11 mL, 24.24 mmol TOP and 0.72 g, 24.30 mmol S) under an inert atmosphere. This mixture was quickly injected into the flask at 350 °C, causing the temperature to drop to 285 °C. After holding the temperature at 350 °C for 8 min, the reaction was air-cooled to 90 °C, and toluene (10 mL) was added.

Purification was performed by alternately precipitating the NRs with methanol (32 mL), centrifuging at 3773 rcf for 5 min, and redispersing in toluene (32 mL) at least three times. The final NR solution was stored in toluene (70 mL). The NR size and shape were measured by TEM. For this purpose, a droplet of the sample in organic solution, preferably chloroform, was deposited on a carbon-coated copper grid and dried in air.

Phase Transfer of CdSe/CdS Nanorods with MPA: The CdSe/CdS nanorods dissolved in toluene were transferred to an aqueous solution using ligand exchange.[36,42] To achieve phase transfer, six times 4.5 mL of the nanoparticle solution was precipitated in 30 mL of a phase-transfer solution (containing methanol [100 mL], MPA [2.6 mL, 29.84 mmol], and KOH [1.14 g, 20.32 mmol]), and the mixture was shaken for 2 h at room temperature in centrifugation vials. After centrifugation (10 min., 8500 rcf), the precipitate was redispersed in 0.1 M aqueous KOH solution (27 mL) which is slightly turbid. And, 1 mL of HCCl$_3$ was added to the aqueous solution (to remove excess ligands and organics) and well shaken. This mixture was again centrifuged for 5 min at 8500 rcf to separate in two phases (HCCl$_3$ at the bottom). Between upper- and lower-phase turbid, yellowish excess of ligands and other organics was accumulated. The upper clear part was very carefully pipetted to another vial for storage. The concentration was determined by atomic absorption spectroscopic (AAS) measurements. The zeta potential of this sample is -35.1 ± 1.9 mV measured by Malvern Zetasizer Nano.

Phase Transfer of CdSe/CdS Nanorods with DMAET: To cover the surface of CdSe/CdS nanorods with DMAET HCl ligands, 25 mL of the previously prepared solution of nanoparticles in toluene was precipitated with methanol and redispersed in chloroform.[36] The solution was mixed with 20 mL of 0.6 M DMAET·HCl solution (20 mL methanol and 1.771 g, 12.50 mmol DMAET·HCl) and shaken. Then, 10 mL of distilled water was added to the two-phase mixture and the mixture was shaken for about 30 min so that all particles were in the aqueous phase. The mixture was centrifuged for 10 min at 3773 rcf. Subsequently, the particles were redispersed in 5 mL of distilled water without further purification for storage. The zeta potential of this sample was $+44.8 \pm 1$ mV.

Preparation of Hydrogels with H$_2$O$_2$: Network formation of CdSe/CdS with MPA ligands triggered by oxidation was carried out with the addition of 39 µL 0.35% H$_2$O$_2$ solution to 1.5 mg Cd (Cd concentration of 3.6 mg mL^{-1} determined by AAS; total solvent volume of 416.7 µL in 0.1 M KOH) within 2 mL Eppendorf reaction tubes.[5] The mixture was well shaken and placed at 80 °C for 1 min in an oven. After around 1 h, the network formation was already visible. The samples were kept for 24 h to form the network structures. To remove byproducts and KOH content, the samples were washed 10 times with ultrapure water. The washing procedure involved careful exchanging the supernatant above the network structure with ultrapure water for 10 cycles. The supernatant was removed using a pipette above the hydrogel surface, and the Eppendorf reaction tube was carefully refilled with ultrapure water. There was a minimum of 1 h between two washing steps to allow the solvent to access the pores from the network. The purified samples were measured in polystyrene cuvettes for spectroscopic investigations.

Preparation of Hydrogels with BaCl$_2$·2H$_2$O or YCl$_3$·6H$_2$O: The CdSe/CdS nanorods with MPA ligands in colloidal solution were gelled by adding 42 µL of 50 mM BaCl$_2$·2H$_2$O (or YCl$_3$6H$_2$O) aqueous solution to 1.5 mg Cd (Cd concentration of 3.6 mg mL^{-1} determined by AAS; total solvent volume of 416.7 µL) nanoparticles in 0.01 M KOH solution within 2 mL Eppendorf reaction tubes.[8,27] To initiate the gelation process homogeneously to the whole sample, the droplet of salt solution (YCl$_3$ or BaCl$_2$) was placed at the wall of the tube above the solution. After closing the tube, it was vigorously shaken and kept at room temperature for 24 h. Network formation was visible within few seconds, as the solution got turbid. To remove byproducts and KOH content, the samples were washed 10 times with ultrapure water. The washing procedure and further handling is described in the section of hydrogel preparation with H$_2$O$_2$.

Preparation of Alcogels with Na$_2$S: Colloidal solutions of CdSe/CdS nanorods with DMAET ligands had a positively charged ligand shell and can be cross-linked by S^{2-} ions. For a typical alcogel preparation, for each gel, 67.5 µL of the as-prepared DMAET-coated NR solution in water was precipitated with acetone within an Eppendorf reaction tube and centrifuged for 5 min at 14 100 rcf. The particles were redispersed in 5 µL ultrapure water and diluted with 410 µL ethanol to obtain a clear solution. To trigger the network formation homogeneously, the process was similar to Ba- and Y-gelation. And, 10.5 µL of a 200 mM Na$_2$S aqueous solution was placed at the wall of the Eppendorf reaction tube and vigorously shaken after closing the tube. The solution got tubid immediately, which indicated the network formation. The samples were kept for 24 h. To remove byproducts, the samples were washed 10 times with ethanol. The washing procedure and further handling was described in the section of hydrogel preparation with H$_2$O$_2$ but with ethanol instead of ultrapure water. Using ethanol was an important step, due to reversible dissolving of the nanoparticle network in water, which could be attributed to the initial bridging via S^{2-} between DMAET ligands.

Preparation of Aerogels: After being washed 10 times with water or ethanol (see hydrogel and alcogel preparation), the solvents of the gel samples were replaced with acetone until no more streaks were visible in the solvent. This was followed by exchanging the solvent to extra dry acetone five times using the same washing procedure (see hydrogels). The resulting acetogel samples were subjected to supercritical drying with liquid CO$_2$ using a critical point dryer (SPI-DRY). To carry out this procedure, the Eppendorf reaction tubes containing the samples were cut above the sample and placed in a transfer vessel from the critical point dryer filled with dried acetone. The liquid acetone was then exchanged with liquid CO$_2$ and flushed for 4–5 min. The sample was left in the autoclave overnight and flushed again with liquid CO$_2$ the following day for 5 min. For the drying process, liquid CO$_2$ was heated to around 36 °C, which was above the critical point at 31 °C and 74 bar. After reaching, the critical phase was slightly released from the autoclave and exchanged to normal air. The resulting aerogel samples were removed from the autoclave and stored under inert gas conditions prior to measurement.

TEM: The samples were dropcasted on carbon-coated copper grids (300 mesh, Quantifoil). Nanoparticle solutions were drop-casted onto the grid from nonpolar solvents (preferably from CHCl$_3$). Gel network structures were prepared from lyogels and aerogels. For lyogels, fragments of the network structures were deposited on the grid by drop-casting. For aerogels, the copper grids were gently pressed against the gel to collect fragments. An FEI Tecnai G2 F20 TMP microscope was used to perform the measurements, which was operated at 200 kV.

SEM: Aerogels were glued on carbon-infiltrated conductive polymer from Plano. SEM images were taken with a JEOL JSM-6700F operated at 2 kV using secondary electron signal and in-lens detector.

Optical Spectroscopy: FLT measurements (time-correlated single-photon counting) were carried out with an Edinburgh FLS 1000 spectrofluorometer irradiated with a 445.1 nm laser LED (2 ms repetition rate) and measured at the maximum emission wavelength of the samples. Decay curves were fitted with monoexponential fit. Emission spectra and PLQYs in absolute mode were measured in an integrating sphere attached to an Horriba DualFL with an excitation wavelength of 445.1 nm.

AAS: To determine the particle concentrations, AAS was performed with a VARIAN AA140 in acetylene/air flame at element specific

wavelength which was 228.8 nm for Cd. Calibration solution concentrations were set to 0, 0.5, 1.0, 1.5, 2.0, and 2.5 mg L^{-1} Cd.

Zeta Potential: All measurements were done in a Malvern Zetasizer Nano. To obtain values from aqueous colloidal solutions for zeta potential, 20 µL of the aqueous solution was diluted in 900 µL corresponding solution (0.1 M KOH for MPA ligand particles or HCl at pH 5 for particles with DMAET) and filled in a DTS1070 folded capillary cell. Zetapotential was measured three times for each sample at 25 °C. Colloidal solutions were stable during measurements without aggregation. Standard derivation was calculated from mean value of the three measurements.

Physisorption: Argon physisorption measurements were performed at 87 K on a 3Flex instrument from micromeritics. The samples (4–12 mg) were activated at mild conditions (25 °C under secondary vacuum for 20 h. For the analysis of the data, the associated software 3Flex Version 5.02 was used. Brunauer–Emmett–Teller (BET)-surface areas were determined by the BET–auto function of the software and total pore volumes were calculated with single-point method at a relative pressure of 0.95 in the adsorption branch. Mercury intrusion measurements were performed on an auto-pore IV instrument from micromeritics using the model 9500. Measurements were taken up to 282 MPa. For the analysis of the data, the associated software micro active 5.0 was used.

Supporting Information

Supporting Information is available from the Wiley Online Library or from the author.

Acknowledgements

Conflict of Interest

The authors declare no conflict of interest.

Data Availability Statement

The data that support the findings of this study are available from the corresponding author upon reasonable request.

Keywords

[1] J. Wang, *Anal. Chim. Acta* **2003**, *500*, 247.

[2] J. L. Mohanan, S. L. Brock, *J. Non-Cryst. Solids* **2004**, *350*, 1.

[3] J. L. Mohanan, I. U. Arachchige, S. L. Brock, *Science* **2005**, *307*, 397.

[4] I. U. Arachchige, S. L. Brock, *J. Am. Chem. Soc.* **2007**, *129*, 1840.

[5] S. Sanchez-Paradinas, D. Dorfs, S. Friebe, A. Freytag, A. Wolf, N. C. Bigall, *Adv. Mater.* **2015**, *27*, 6152.

[6] B. Cai, V. Sayevich, N. Gaponik, A. Eychmüller, *Adv. Mater.* **2018**, *30*, 1707518.

[7] P. Rusch, B. Schremmer, C. Strelow, A. Mews, D. Dorfs, N. C. Bigall, *J. Phys. Chem. Lett.* **2019**, *10*, 7804.

[8] M. Rosebrock, D. Zámbó, P. Rusch, D. Pluta, F. Steinbach, P. Bessel, A. Schlosser, A. Feldhoff, K. D. J. Hindricks, P. Behrens, D. Dorfs, N. C. Bigall, *Adv. Funct. Mater.* **2021**, *31*, 2101628.

[9] D. Zámbó, A. Schlosser, R. T. Graf, P. Rusch, P. A. Kißling, A. Feldhoff, N. C. Bigall, *Adv. Opt. Mater.* **2021**, *9*, 2100291.

[10] M. Rosebrock, D. Zámbó, P. Rusch, R. T. Graf, D. Pluta, H. Borg, D. Dorfs, N. C. Bigall, *Small* **2023**, *19*, 2206818.

[11] A. Figuerola, I. R. Franchini, A. Fiore, R. Mastria, A. Falqui, G. Bertoni, S. Bals, G. Van Tendeloo, S. Kudera, R. Cingolani, L. Manna, *Adv. Mater.* **2009**, *21*, 550.

[12] S. K. Gill, L. J. Hope-Weeks, *Chem. Commun.* **2009**, *29*, 4384.

[13] S. K. Gill, P. Brown, L. J. Hope-Weeks, *J. Sol-Gel Sci. Technol.* **2011**, *57*, 68.

[14] P. Li, A. Lappas, R. Lavieville, Y. Zhang, R. Krahne, *J. Nanopart. Res.* **2012**, *14*, 978.

[15] T. Hendel, V. Lesnyak, L. Kühn, A.-K. Herrmann, N. C. Bigall, L. Borchardt, S. Kaskel, N. Gaponik, A. Eychmüller, *Adv. Funct. Mater.* **2013**, *23*, 1903.

[16] L. Nahar, R. J. A. Esteves, S. Hafiz, U. Oezguer, I. U. Arachchige, *ACS Nano* **2015**, *9*, 9810.

[17] R. Wendt, B. Märker, A. Dubavik, A.-K. Herrmann, M. Wollgarten, Y. P. Rakovich, A. Eychmüller, K. Rademann, T. Hendel, *J. Mater. Chem. C* **2017**, *5*, 10251.

[18] A. Schlosser, L. C. Meyer, F. Lübkemann, J. F. Miethe, N. C. Bigall, *Phys. Chem. Chem. Phys.* **2019**, *21*, 9002.

[19] J. L. Davis, K. L. Silva, S. L. Brock, *Chem. Commun.* **2020**, *56*, 458.

[20] F. Lübkemann, J. F. Miethe, F. Steinbach, P. Rusch, A. Schlosser, D. Zámbó, T. Heinemeyer, D. Natke, D. Zok, D. Dorfs, N. C. Bigall, *Small* **2019**, *15*, 1902186.

[21] A. Freytag, S. Sánchez-Paradinas, S. Naskar, N. Wendt, M. Colombo, G. Pugliese, J. Poppe, C. Demirci, I. Kretschmer, D. W. Bahnemann, P. Behrens, N. C. Bigall, *Angew. Chem., Int. Ed.* **2016**, *55*, 1200.

[22] D. Müller, D. Zámbó, D. Dorfs, N. C. Bigall, *Small* **2021**, *17*, 18.

[23] N. Gaponik, A. Wolf, R. Marx, V. Lesnyak, K. Schilling, A. Eychmüller, *Adv. Mater.* **2008**, *20*, 4257.

[24] F. Matter, A. L. Luna, M. Niederberger, *Nano Today* **2020**, *30*, 100827.

[25] V. Lesnyak, A. Wolf, A. Dubavik, L. Borchardt, S. V. Voitekhovich, N. Gaponik, S. Kaskel, A. Eychmueller, *J. Am. Chem. Soc.* **2011**, *133*, 13413.

[26] R. Du, Y. Hu, R. Hübner, J.-O. Joswig, X. Fan, K. Schneider, A. Eychmüller, *Sci. Adv.* **2019**, *5*, aaw4590.

[27] D. Zámbó, A. Schlosser, P. Rusch, F. Lübkemann, J. Koch, H. Pfnür, N. C. Bigall, *Small* **2020**, *16*, 1906934.

[28] L. Altenschmidt, S. Sánchez-Paradinas, F. Lübkemann, D. Zámbó, A. M. Abdelmonem, H. Bradtmüller, A. Masood, I. Morales, P. de la Presa, A. Knebel, M. A. G. García-Tuñón, B. Pelaz, K. D. Hindricks, P. Behrens, W. J. Parak, N. C. Bigall, *ACS Appl. Nano Mater.* **2021**, *4*, 6678.

[29] P. Rusch, D. Zámbó, N. C. Bigall, *Acc. Chem. Res.* **2020**, *53*, 2414.

[30] J. Schlenkrich, D. Zámbó, A. Schlosser, P. Rusch, N. C. Bigall, *Adv. Opt. Mater.* **2022**, *10*, 2101712.

[31] A. Schlosser, J. Schlenkrich, D. Zámbó, M. Rosebrock, R. T. Graf, G. Escobar Cano, N. C. Bigall, *Adv. Mater. Interfaces* **2022**, *9*, 2200055.

[32] D. Wen, A. K. Herrmann, L. Borchardt, F. Simon, W. Liu, S. Kaskel, A. Eychmüller, *J. Am. Chem. Soc.* **2014**, *136*, 2727.

[33] M. Artemyev, E. Ustinovich, I. Nabiev, *J. Am. Chem. Soc.* **2009**, *131*, 8061.

[34] S. F. Wuister, I. Swart, F. van Driel, S. G. Hickey, C. de Mello Donegá, *Nano Lett.* **2003**, *3*, 503.

[35] A. L. Rogach, T. Franzl, T. A. Klar, J. Feldmann, N. Gaponik, V. Lesnyak, A. Shavel, A. Eychmüller, Y. P. Rakovich, J. F. Donegan, *J. Phys. Chem. C* **2007**, *111*, 14628.

[36] T. Kodanek, H. M. Banbela, S. Naskar, P. Adel, N. C. Bigall, D. Dorfs, *Nanoscale* **2015**, *7*, 19300.

[37] M. Abdellah, S. Zhang, M. Wang, L. Hammarström, *ACS Energy Lett.* **2017**, *2*, 2576.

[38] M. Micheel, B. Liu, M. Wächtler, *Catalysts* **2020**, *10*, 1143.

[39] J. Ding, Z. Lian, Y. Li, S. Wang, Q. Yan, *J. Phys. Chem. Lett.* **2018**, *9*, 4221.

[40] L. Carbone, C. Nobile, M. De Giorgi, F. D. Sala, G. Morello, P. Pompa, M. Hytch, E. Snoeck, A. Fiore, I. R. Franchini, M. Nadasan, A. F. Silvestre, L. Chiodo, S. Kudera, R. Cingolani, R. Krahne, L. Manna, *Nano Lett.* **2007**, *7*, 2942.

[41] W. W. Yu, L. Qu, W. Guo, X. Peng, *Chem. Mater.* **2004**, *16*, 560.

[42] H. G. Bagaria, E. T. Ada, M. Shamsuzzoha, D. E. Nikles, D. T. Johnson, *Langmuir* **2006**, *22*, 7732.